Article

Not peer-reviewed version

Irradiation Characteristics of Non-impregnated Micropore Graphite for Use in Molten Salt Nuclear Reactors

Pengfei Lian , Pengda Li , Hefei Huang * , Jinliang Song * , Zhongfeng Tang , Zhanjun Liu *

Posted Date: 15 April 2024

doi: 10.20944/preprints202404.0876.v1

Keywords: non-impregnated graphite; irradiation performance; microstructure; defect evolution; molten salt reactor

Article

Irradiation Characteristics of Non-Impregnated Micropore Graphite for Use in Molten Salt Nuclear Reactors

Pengfei Lian [1,2,†], Pengda Li [2,3,†], Hefei Huang [2,*], Jinliang Song [2,4,*], Zhongfeng Tang [2,4] and Zhanjun Liu [1,4,*]

[1] Key Laboratory of Carbon Materials, Institute of Coal Chemistry, Chinese Academy of Sciences, Taiyuan 030001, China.
[2] Shanghai Institute of Applied Physics, Chinese Academy of Sciences, Shanghai 201800, China.
[3] University of Chinese Academy of Sciences, Beijing 100049, China.
[4] Dalian National Laboratory for Clean Energy, Dalian 116023, China.
* Correspondence: huanghefei@sinap.ac.cn (H.H.); jlsong1982@yeah.net (J.S.); zjliu03@sxicc.ac.cn (Z.L.); Tel./Fax: +86-21-39194258
† The two authors contributed equally to this study and shared the first authorship.

Abstract: Non-impregnated small pore graphite (NSPG) with the compact microstructure for using in molten salt reactors (MSR) was prepared by the novel process, and the pore diameter of the obtained graphite was reduced to ~800 nm. The irradiation evaluation of the prepared graphite was carried out by 7 MeV Xe^{26+} ion irradiation and the microstructural changes of the graphite were investigated with IG-110 as a comparison. The graphitization degree of NSPG was higher than that of IG-110, though it was not subjected to an impregnation process. Under low-dose ion irradiation (<2.5 dpa), the microscopic morphology of the NSPG changes in a small magnitude, and the lamellar structure of graphite remains within the scale of more than a dozen nanometers, which exhibits a better resistance to irradiation. With the increase of irradiation dose, the accumulation of defects leads to graphite toward amorphization, which shows consistency with IG-110. This study provides an efficient and low-cost method for the preparation of graphite for MSR, and investigates the damage behavior of graphite, which is of great significance in accumulating data for the development of MSR nuclear graphite and the optimal design of graphite materials.

Keywords: non-impregnated graphite; irradiation performance; microstructure; defect evolution; molten salt reactor

1. Introduction

Molten salt reactor (MSR) is one of the candidate types of Generation IV advanced nuclear energy systems with the advantages of high-intrinsic safety, low nuclear waste, excellent economics, compatibility and suitability for small modular designs [1]. Graphite is the most critical structure and moderator material in MSR, requires pore sizes of less than 1 μm to prevent the penetration of molten fluoride salts [2]. In order to reduce the pore size of graphite, researchers have proposed a number of methods in designing the molten salt breeder reactor (MSBR), including: impregnating graphite with hydrocarbons, pre-filling the surface pores of graphite with molten salts, and impregnating or sealing the surface pores of graphite with pyrolysis gases [3] However, the lowest permeability of 10^{-8} cm^2/s not achieved by hydrocarbon impregnation; pre-filling with molten salts was only cursorily investigated; the irradiation resistance of graphite impregnated with pyrolysis gas was poor; the surface sealing treatment failed due to the mismatch between the coating and the graphite substrate [4] Recently, based on the results of previous research, the techniques to improve the permeability of graphite have been further developed. These include: 1. sealing of existing nuclear graphite (e.g., IG-

 doi:10.20944/preprints202404.0876.v1

110) with PyC, glassy carbon, SiC coatings, and various composite coatings [5–8]; 2. impregnation of graphite with phenolic resins, phenol-formaldehyde, and polyimide [6,9]; 3. development of new types of graphite with very low porosity or non-binder graphite [10,11]. All of these have been proven to be successful in preventing the penetration of molten salt. However, the vapor deposition method and vapor infiltration process require time and cost consuming, and also can lead to spatial gradients [12], resulting in poor uniformity and irradiation properties [13,14]. The non-binder graphite (such as NPIG and SSNG) are prone to cracking due to the large contraction of the carbonization process [15], making it difficult to prepare large scale products. In addition, some novel graphites demonstrated the higher irradiation sensitivity in ion irradiation experiments [13,14,16–18].

Therefore, for the design and construction of molten salt reactors, the development of graphite that can prevent molten salt infiltration is crucial. It is important to note that the uniformity of the graphite determines the safety, lifetime and cost of the MSR. However, the present small pore graphite was prepared by multiple pitch impregnation process leading to the huge differences in the structures and properties between internal and external of the graphite, which causes the difficulties in reactor design and irradiation experiments, and also increases the cost and production cycle of graphite. In this paper, a novel type of non-impregnated small pore-size graphite (NSPG) with the average pore size of ~800 nm is prepared by liquid-phase slurry coating with organic solvents on the coke surface to realize the pitch binder uniformly covering the aggregate cokes. NSPG does not require the additional impregnation process and possesses the advantages of low cost, short production cycle, performance uniformity, high pass-rate of production, etc. The in-service behavior of NSPG in the reactor irradiation environment should be different from that of other graphite. Therefore, the low cost pre-neutron irradiation screening is required to provide the data needed for reactor design and evaluation, and to determine whether the irradiation resistant of the obtained graphite is close to that of traditional nuclear graphite for the next step in the scaling-up process and performance tuning. However, the experimental setups for neutron irradiation are few and expensive. Heavy ion irradiation has the advantages of being controllable, efficient, cost-effective, and low residual radioactivity, which is often used to simulate neutron irradiation to evaluate the response of graphite. 7 MeV Xe^{26+} irradiation has been widely used to simulate neutron irradiation in recent years and has been used to study the irradiation behavior of new types of graphite, such as coating, resin-impregnated graphite, NPIG and SSNG [13,14,16,18–20].It is worth noting that ions damage the microstructure of nuclear graphite at a much greater rate than neutrons, and the experimental results at room temperature are more limited. In addition, ions have a very limited range (micrometers) in graphite, whereas neutrons can penetrate centimeter-sized graphite samples. Thus, ion irradiation is limited to understanding certain aspects of the behavior of graphite. This paper focuses on the effect of ion irradiation on the microstructure in graphite surfaces. The reference nuclear graphite for evaluating the irradiation performance of graphite for MSR was chosen as IG-110 (Toyo Tanso Co, Ltd.), because IG-110 has already been maturely applied in many reactors, such as HTR-PM and HTR-10, and has accumulated a wealth of data by completing many irradiation experiments.

This study aims to prepare the NSPG and investigate its irradiation behaviors using 7 MeV Xe^{26+} to verify the irradiation stability and assess the suitability of the new graphite. The surface morphology changes and defect formation of graphite after irradiation were evaluated to improve the understanding of the irradiation behavior of the graphite.

2. Experimental

2.1. Sample Preparation

NSPG was prepared by the mixed fillers of microcrystalline graphite (purified at high temperature) with an average particle size of 12 μm and petroleum cokes as fillers. The binder used was coal tar pitch and the solvent selected was tetrahydrofuran. The fillers and pitch mixed in tetrahydrofuran were blended in a mixer at 60 ºC with a mixing time of 60 minutes. The mixed materials were dried at 100 °C for 4 h to ensure the complete removal of the solvent, followed by pulverization into

 doi:10.20944/preprints202404.0876.v1

fine particles. These particles were formed to cylindrical green bodies under 200 MPa with diameters about 80 mm and a thickness about 80 mm through isostatic pressing. These molded bodies were subjected to calcination at 1000 °C for 3 h with a heating rate of 10 °C/h in a nitrogen atmosphere. Finally, the secondary calcination and graphitization processes were completed in an argon environment at a temperature of about 2900 °C with a heating rate of 100 °C/h for the preparation of NSPG.

The NSPG specimens were cut into 5.0×5.0×1.0 mm^3 pieces for Xe^{26+} irradiation. All samples were polished and ultrasonically cleaned before irradiation. Subsequently, the specimens were separated from each other in 5 groups (a, b, c, d and e). Non-treated specimens (group e) were retained for comparative purposes. The following radiation studies were performed with the smooth surface of graphite.

2.2. Ion Irradiation

The samples were irradiated at the 320 kV integrated research platform of the Institute of Modern Physics, Chinese Academy of Science, at room temperature with 7 MeV Xe^{26+} ion beams. Before performing the ion beam irradiation, information such as the deposition depth of the ion beam in the graphite sample and the irradiation damage distribution were determined by SRIM simulations. As calculated by SRIM, the irradiation depth was ~2.9 μm, and the irradiation damage reached the maximum at a depth of ~2.3 μm. The damage level (displacement per atom, dpa) was calculated by $dpa = \frac{N_{displacement}}{N_{atom}} = \frac{\Phi n_{displacement}}{\rho_{atom}}$, where Φ, $n_{displacement}$, ρ_{atom} are the ion fluence, the number of displacements/ion/unit depth, and the atomic density, respectively [16]. Table 1 shows the fluences and corresponding irradiation damage level of the ion irradiation experiments. Figure 1 gives the depth profiles of the displacement damage.

Table 1. Fluences and corresponding irradiation damage doses of ion irradiation experiments of NSPG.

Fluence (ions/cm^2)	Peak irradiation dose (dpa)	Surface irradiation dose (dpa)
9.6×10^{13}	0.1	0.02
4.8×10^{14}	0.5	0.11
2.4×10^{15}	2.5	0.55
4.8×10^{15}	5.0	1.25

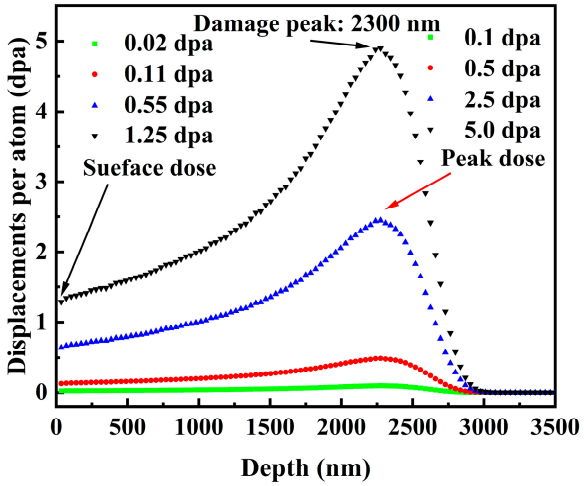

Figure 1. Depth profile of displacement induced by 7 MeV Xe^{26+} ion irradiation in graphite as simulated with SRIM.

 doi:10.20944/preprints202404.0876.v1

2.3. Characterization Methodology

The information of the pore structure of NSPG was obtained by automatic mercury porosimeter (AutoPore IV 9500) as follows: The porosity is the ratio of the volume of measurable pores and voids in a solid to the total volume occupied by the solid. Mercury porosimetry is also based on this principle [21]: $\Phi = \frac{V_1}{V_2}$. The V_1 and V_2 in the equation are the volume of mercury pressed in at low and high pressures and the volume of the sample, respectively. V_1 was measured directly in the low and high pressure experiments, most critically to obtain the sample volume V_2. The details are as follows [21]: $V_2 = \frac{W_4 - [W_3 - (W_2 - W_1)]}{\rho_{Hg}}$. W_1, W_2, W_3 and W_4 are the mass of the blank sample tube, the total mass of the blank sample tube and the sample, the total mass of the blank tube, sample and injected mercury at a certain pressure, the total mass of the blank sample tube and the mercury that filled the blank sample tube, respectively. The bulk density is the weight per unit volume in the natural state (including the solid material together with its open and closed pores). It can be calculated from the following formula: $\rho_0 = \frac{M}{V_0}$. The M and V_0 in the equation are the quality of the material, the volume of the material, respectively. It can also be calculated using the volume of mercury discharged from the sample at the minimum mercury filling pressure. The results of the two calculations are about the same. The pore diameter can be obtained from Washburn equation by means of the applied pressure [22]: $\delta = -\frac{4\gamma \cos\theta}{P}$. The δ, γ, P and θ in the equation are the median pore diameter of graphite, the surface tension of mercury (0.485 N/m), the pressure and contact angle of mercury with graphite (130°), respectively [22]. However, the mercury porosimetry has certain limits in that it is built on the assumption of the pores of graphite that can be regarded as cylinders. In addition, when the applied pressure exceeds approximately 18.2 MPa, the pores of the graphite internals may be locally deformed or damaged, resulting in high measured porosity [23]. Despite this, mercury porosimetry is still widely used for the measurement of pore size of graphite.

The changes in the morphological structure of the graphite samples were monitored by scanning electron microscopy (SEM) (LEO 1530VP). The samples were vertically scanned along the surface of the graphite with the secondary electron (SE2) mode at an accelerating voltage of 5 kV. Morphological changes at the same location of the samples were monitored and observed comparatively before and after irradiation to reveal the effect of irradiation on the samples.

To quantify the irradiation-induced changes in the micromorphology and structure of the surface of NSPG, the samples were analyzed by atomic force microscopy (AFM) (Bruker Multimode 8) before and after irradiation. The imaging mode is selected to be non-contact, the scanning resolution of 512 pixels × 512 pixels, and post-processing of the data is accomplished with the help of NanoScope Analysis.

The grazing incidence XRD (GIXRD) was carried out by a Bruker D8 Advance powder X-ray diffraction (XRD) utilizing a CuKα1 radiation source (λ=1.5406 Å) conditioned by two 2.5° Soller slits and a 0.025 mm Ni mask. The reflected X-ray intensity was continuously measured and recorded with a LynxEye XE counter during θ~2θ scans, which were conducted within the range of 20~70° (2θ), under a tube power setting of 40 kV/40 mA. These scans were executed with a step size of 0.02° (2θ) at 0.15 s intervals. The angle of incidence is set to 0.2° to decrease the effects of the sample's unirradiated area.

A Raman spectrometer (Horiba Jobin-Yvon LabRam HR800) was used to characterise the defects induced by irradiation. In this study, an excitation wavelength of 532.0 nm and a grating of 600 gr/mm were used. The effective depth of penetration was about 50.0 nm. The Raman microscope used in this study has a spatial resolution of approximately 400 nm and is equipped with a 1024×640 pixel CCD camera. The spectral resolution was 1.5 cm^{-1} and the wavenumber accuracy was 1 cm^{-1}. The excitation source is a green line of an argon laser. The laser was focused at different magnifications on the surface of the sample using a Zeiss LD EC Epiplan-Neofluar objective.

 doi:10.20944/preprints202404.0876.v1

3. Results and Discussion

3.1. Pore structure Analysis

The pore size distribution of NSPG and IG-110 and the relationship curves between mercury injection and pressure are shown in Figure 2. Table 2 provides the properties of NSPG and IG-110. The density and open porosity of NSPG were 1.79 g/cm^3 and 15.9%, respectively. While the density and open porosity of IG-110 were 1.77 g/cm^3 and 18.4%, respectively. In addition, the median pore diameter of NSPG is 0.802 μm. This is much smaller as compared to the 1.84 μm of IG-110. The process of the incremental injection of mercury into the graphite shown in Figure 2b can be divided into three parts. In the case of the IG-110, only a small amount of mercury penetrates into graphite at the first stage pressure (0~5.09×10^5 Pa). But with pressure increase, mercury injection started to increase sharply in the second stage from 5.09×10^5 Pa to 1.99×10^7 Pa and then tended to saturate. In the third stage, when the pressure is greater than 1.99×10^7 Pa, mercury injection continues to increase may be due to the closed cell mechanical break. The mercury injection process of NSPG can also be similarly divided into three such stages. The differences between NSPG and IG-110 are mainly reflected in the triggering and saturating pressures, which are caused by the pore size. Because the smaller pore structure of NSPG will produce a higher interface capacityforce, the first mercury penetration stage will slowly continue to 1.18×10^6 Pa. In addition, due to the lower open porosity of NSPG, the total amount of final mercury injected (0.0898 ml/g) is much less than IG-110 (0.1045 ml/g). The results indicate that IG-110 is unable to inhibit the penetration of molten salts, whereas NSPG can meet the pore size requirements of MSRs.

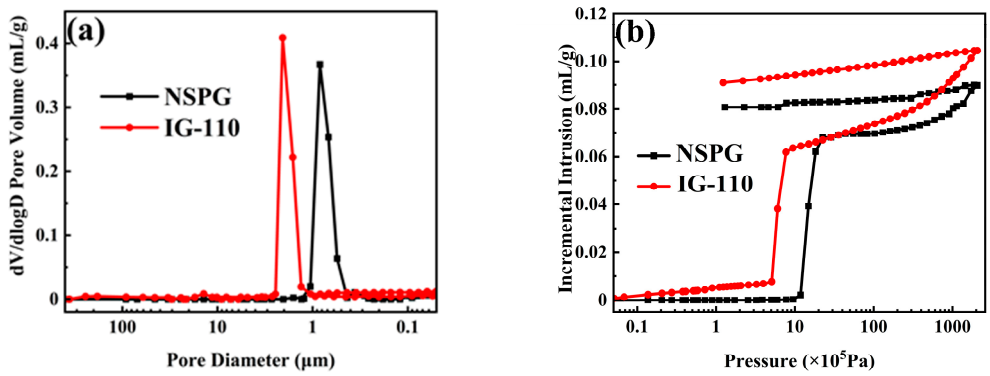

Figure 2. The pore size distribution of NSPG and IG-110 (a) and the relationship curves between mercury injection and pressure (b).

Table 2. Properties of NSPG and IG-110 [11] graphite.

Properties	IG-110	NSPG
Bulk density (g/cm^3)	1.77 ± 0.02	1.79 ± 0.02
Open porosity (%)	18.4 ± 0.1	15.9 ± 0.1
Median pore diameter (volume,μm)	1.840	0.802
Flexure strength (MPa)	39.2 ± 2.5	61.0 ± 2.5
Compressive strength (MPa)	78 ± 3	102 ± 3
Thermal conductivity (W/m·K)	116± 2	127± 2
CTEs (25-300 °C, 10^{-6}/K)	4.5 ± 0.2	4.1 ± 0.2

 doi:10.20944/preprints202404.0876.v1

3.2. Morphology Variation

The SEM images of NSPG and IG-110 were shown in Figure 3(a) and 3(b). The graphite before irradiation all shows the typical surface morphology after polishing of polycrystalline graphite, especially IG-110 exists many pores and fine graphite microcrystalline structure, the shape of these pores is irregular, and the distribution of pore size is wide, with the size ranging from a few μm to tens of μm. In contrast, the surface of the NSPG is relatively smooth, with fewer and smaller pores. The edges and interiors of the pores of NSPG are smooth and flat, and there are almost no significant cracks. This is in agreement with the results of the mercury injection penetration test, which indicate that although NSPG is not subjected to an impregnation process, the smaller pore structure can satisfy the infiltration requirements of graphite for molten salt reactors.

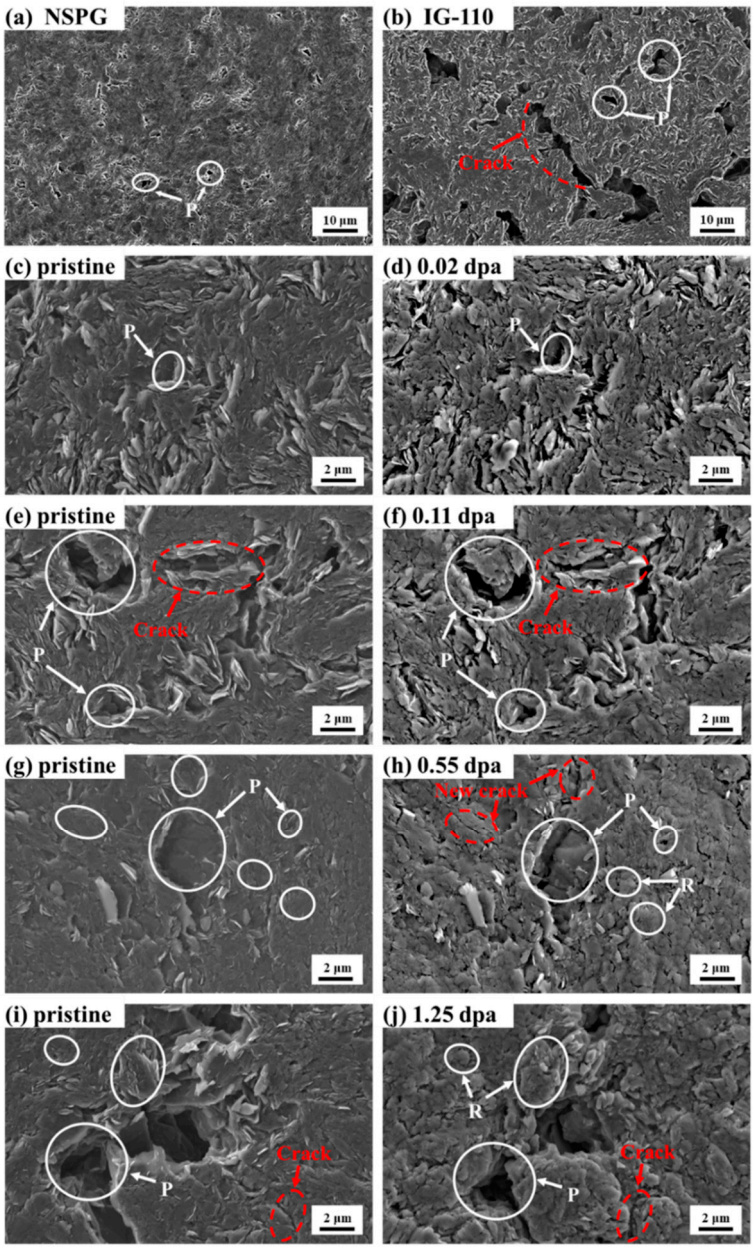

Figure 3. SEM images of NSPG (a, c, e, g and i) and IG-110 (b) before and after irradiation at surface damage dose of 0.02 dpa (d), 0.11 dpa (f), 0.55 dpa (h) and 1.25dpa (j). (P and R refer to pores and ridge-like structures, respectively).

After different doses of Xe ion irradiation at room temperature, significant changes in the morphology of the surface of NSPG could be observed in the SEM images shown in Figure 3(c~j). As the irradiation dose increases, the flatness of the graphite surface gradually deteriorates (Figure 3d,

 doi:10.20944/preprints202404.0876.v1

f, h, i). After the lower irradiation dose (0.02~0.11 dpa), the wrinkles on the graphite surface are more distinct and the surface becomes rough, which is associated with the irradiation-induced c-axis swelling [24]. This is because the incident Xe ions bombard carbon atoms from graphite lattice nodes during irradiation, generating a large number of interstitial atoms and vacancies. The accumulation of interstitial atoms between the two basal planes as well as the growth of incomplete planes result in the formation of additional basal planes and interstitial rings, which result in the expansion of graphite microcrystals along the c-axis direction. At the same time, the pores of graphite showed the phenomenon of squeezing and contracting after irradiation with the low dose of irradiation, and the average size and density of pores on the surface of graphite are reduced, which is due to the fact that the pores and microcracks of graphite have an absorptive effect on the swelling of the graphite microcrystals, but this absorptive effect has a limitation, for example, under 0.11 dpa irradiation (Figure 3f), the pores of the graphite surface will tend to be closed when the absorptive effect of the graphite surface swelling reaches the saturation level. Previous studies have shown that the dimensional change of graphite is faster at irradiation temperatures below 250 °C, whereas in this paper the irradiation is carried out at room temperature, thus the amorphization of graphite will be rapidly induced [25]. Heggie et al. pointed out that permanent basal plane nano-buckling may also lead to the expansion of the c-axis of graphite crystals at irradiation temperatures below 250 °C [26]. So at the higher dose of irradiation (0.55 dpa), the surface of graphite produced obvious bulging protrusions, i.e., the “Ridge-like” structure (Figure 3h), which was mainly caused by: firstly, the increase in the degree of swelling induced by irradiation, and secondly the pores of graphite reach saturation in the absorption of swelling. It is noteworthy that after 0.55 dpa irradiation, the surface of NSPG also showed small cracks, which is due to the increased expansion of graphite microcrystals in the c-axis direction leading to dimensional shrinkage in the a-axis direction. With the increase of the surface irradiation dose to 1.25 dpa, the surface morphology of NSPG changed greatly, and the increase of the size of the “ridge-like” structure and the growth of cracks were more obvious. The relative position of graphite flakes also shifted, and the boundary bending and deformation, which was similar to that of IG-110 (Figure 4d) [20]. This indicates that Xe ion bombardment has led to the destruction of the microstructure of the graphite surface, and the irradiation damage effect is more obvious. But compared with the traditional nuclear graphite IG-110 at the same irradiation dose (Figure 4b), the surface of NSPG is relatively intact with less change, which indicates that NSPG has a certain resistance to irradiation in terms of micro-morphology. Additionally, in marked contrast to NSPG, the wrinkled surface of IG-110 becomes relatively smooth after irradiation, which may be related to the initial crystallinity of graphite. Previous studies have shown that this may be due to the improvement of crystal orientation of the disordered structure by irradiation-induced graphitization [20].

To visualize the irradiation-induced “ridge-like” structure and to quantitatively observed the irradiation-induced c-axis swelling, the 3D morphology and surface roughness changes of the samples before and after irradiation are shown in Figure 5. The results show that the roughness of the sample surface increases rapidly after irradiation at low irradiation doses (0.02~0.11 dpa), which directly leads to wrinkles on the sample surface being more prominent, consistent with the results observed in SEM images. As the surface irradiation dose increases (Figure 5d, e), the roughness of the surface of samples continues to increase, while the number and size of “ridge-like” structures increase, forming the larger protruding particles and generating the “bulging” phenomenon, which is related to the absorption of irradiation-induced swelling by the pores and cracks of graphite reaching saturation, resulting in a more pronounced increase in expansion in the vertical direction, so that the SEM observed a huge change in the morphology of samples, and AFM supplemented this from different perspectives, which corresponds to the SEM results.

Preprints.org (www.preprints.org) | NOT PEER-REVIEWED | Posted: 15 April 2024 doi:10.20944/preprints202404.0876.v1

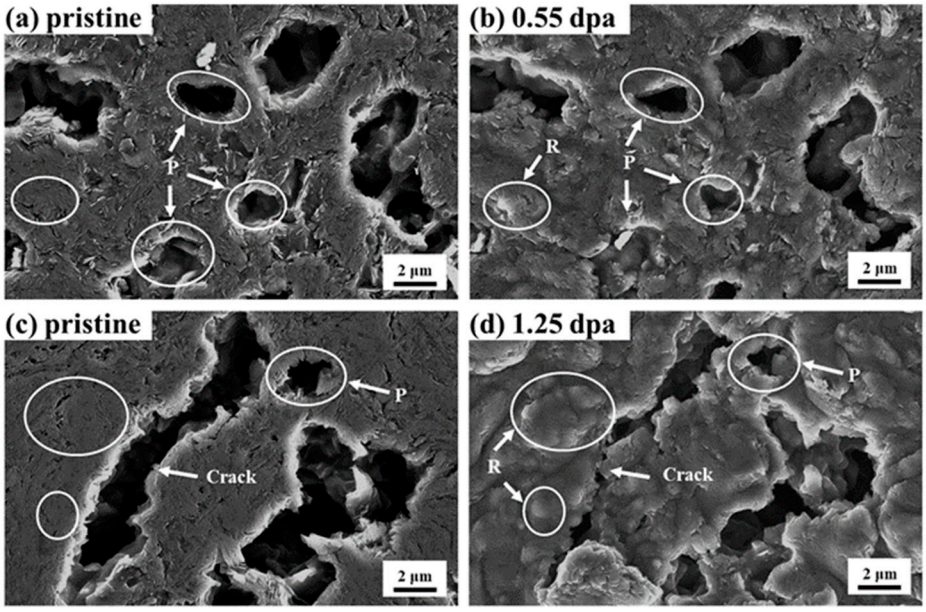

Figure 4. SEM images of IG-110 pristine (a) (c)and after irradiation at surface damage dose of 0.55dpa(b), 1.25dpa (d) [20].

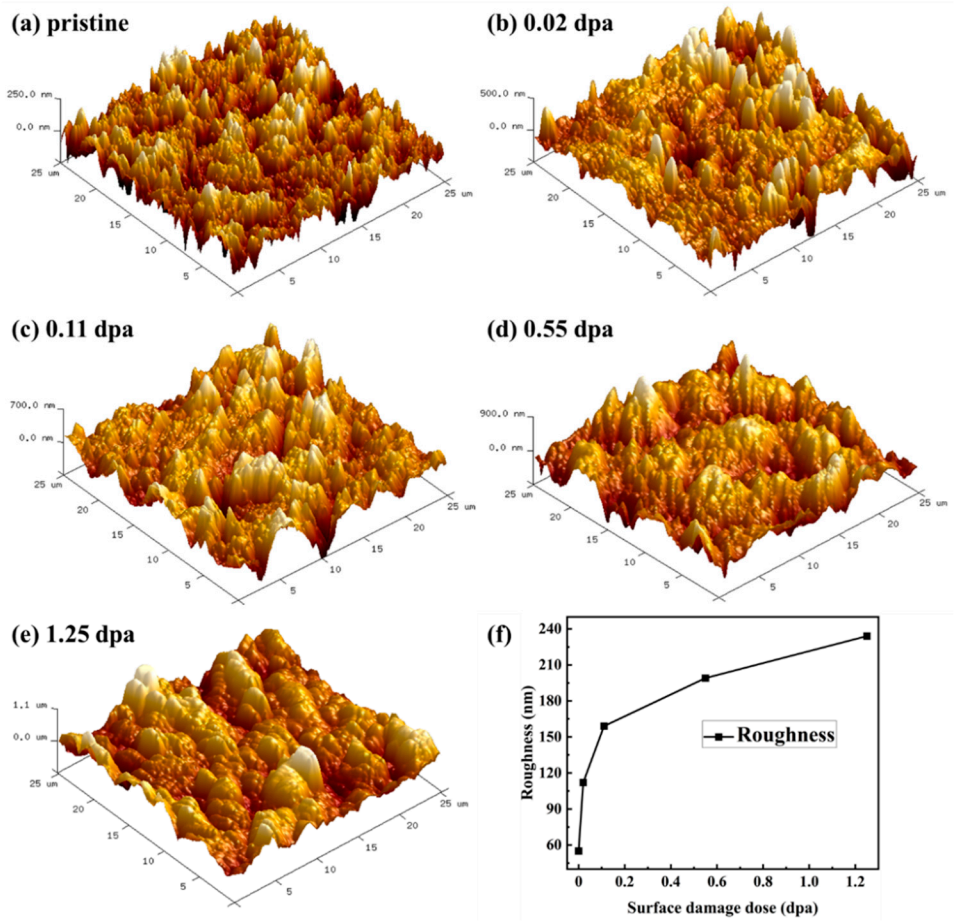

Figure 5. AFM images of NSPG before (a) and after irradiation at surface damage dose of (b) 0.02 dpa, (c) 0.11 dpa, (d) 0.55 dpa and (e) 1.25 dpa; (f) Roughness of NSPG varies with surface damage dose.

 doi:10.20944/preprints202404.0876.v1

3.3. Structural Variation

The XRD patterns in Figure 6 show that the prepared NSPG and IG-110 have the same hexagonal structure (graphite-2H: hexagonal, space group P63/mmcP63/m2/m2/c). The (002) and (004) diffraction peaks in the figure are related to the graphitized structure of the materials, which indicates that both graphites have the ordered graphite structure. The Braggs diffraction angle of the (002) diffraction peak of NSPG is a little larger as compared to IG-110. The d_{002} (interlayer spacing), crystallite stacking height (L_c) and the graphitization degree (g) can be calculated by referring to the following equation [27]: $d_{002} = \frac{\lambda}{2sin\theta}$, $g = \frac{0.3440 - d_{002}}{0.3440 - 0.3354}$ and $L_c = \frac{0.89\lambda}{\beta_{002} cos\theta_{002}}$, respectively. As calculated, NSPG has a smaller layer spacing and higher graphitization, with a graphitization of 89.77%, which is larger than that of IG-110 at 83.60%, and this difference in the degree of initial graphitization will influence the irradiation behavior of the graphite.GIXRD patterns and (002) peaks of NSPG graphite before and after irradiation are shown in Figure 6c. Figure 6c shows clearly that the (002) diffraction peak of irradiated NSPG shift to lower diffraction angles, which is similar to IG-110 [20]. This indicates an increase of d_{002} and a decrease of the graphitization degree of NSPG. Figure 6d shows the changing trend of d_{002} and crystallite stacking height (L_c) of NSPG with irradiation dose. The d_{002} of NSPG increased as the irradiation dose increased and reached the saturation at a dose of 2.5 dpa, whereas L_c increased rapidly after irradiation at a dose of 0.1 dpa, but decreased at 0.5 dpa, and then stabilized with dose, this trend of L_c is similar to that of the data from neutron irradiated nuclear graphite [28]. These are caused by the displacement damage cascade resulting from irradiation, which produces a large number of point defects in the graphite, which further migrate and merge to develop into dislocations, and the dislocations climb to form new planes, leading to an increase in the layer spacing of the graphite as well as expansion of the c-axis [29]. The decrease of L_c is related to the irradiation-induced disordered structure, with further increase of irradiation dose, the strain during irradiation induces bending of the basal plane, fracture of the grain surface and fragmentation of the grains, i.e. the accumulation of defects produced by irradiation leads to the development of graphite towards amorphization. The appearance of " ridge-like" structures can be considered as an intermediate stage in the amorphization of the surface of graphite [18]. The XRD results provide evidence for the SEM results that the irradiation-induced changes in the microstructure of graphite caused the morphology changes in section 3.2.

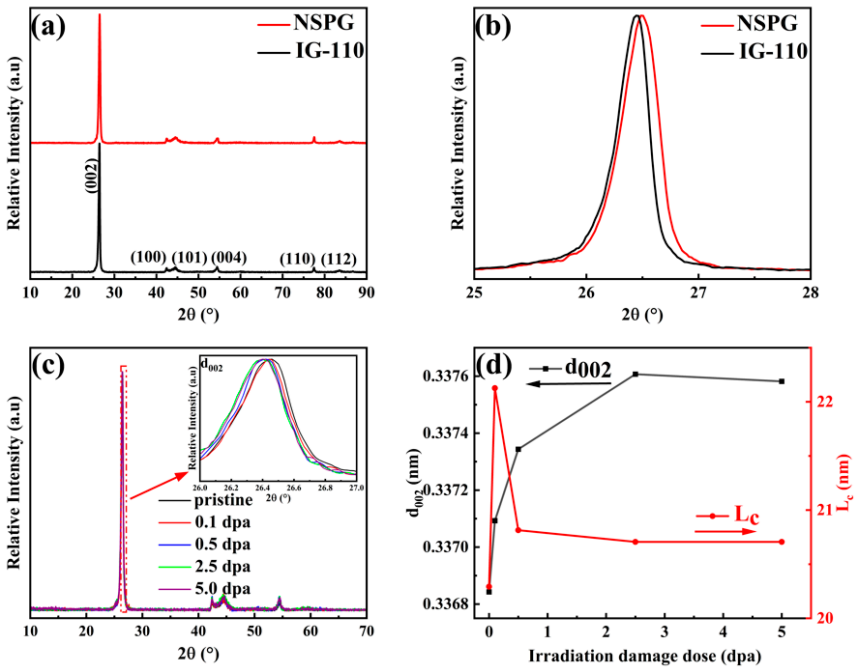

Figure 6. XRD patterns (a, b) of pristine NSPG and IG-110; (c) GIXRD patterns of NSPG and irradiated NSPG; (d) d_{002} and L_c as functions of irradiation dose.

 doi:10.20944/preprints202404.0876.v1

Raman spectroscopy is a common technique for analyzing carbon materials such as graphite, carbon fibers, carbon nanotubes and fullerenes. In the case of highly ordered graphitic materials, the G peak (near 1580 cm^{-1}) is the intrinsic peak of graphite, which is Raman-active for sp^2 hybridization. The D peak (near1350 cm^{-1}) represents the disorder of the graphitic structure, which is associated with vacancy defects, edge disorder, and irregular C (sp^3 bonds), etc. [30]. The changes of graphite grain size and disorder induced by irradiation can be indirectly obtained by analyzing certain parameters of the characteristic peaks, such as peak shape, intensity or full width half maximum (FWHM), etc. The I_D/I_G intensity ratio is an important parameter to quantify the disorder, and it has been widely used to characterize the density of defects in graphite materials. The grain size L_a can be calculated from the *T-K* empirical formula [31]: $L_a(nm) = (2.4 \times 10^{-10})\lambda^4(\frac{I_D}{I_G})^{-1}$, where λ(nm) is the wavelength of the laser, which is 532 nm in this work, and this formula is valid for use in the range of L_a>2 nm. Figure 7(a) and (b) are the Raman spectra of NSPG before and after irradiation, respectively. To further investigate the effect of irradiation dose on the microstructure of graphite, the Raman spectra of NSPG were fitted to the peaks according to Lorentz principle and divided into 1150, 1350, 1500, and 1580 cm^{-1}, which are denoted as v_1, D, G, and v_3 peaks. The v_1 peak is a mixed vibration of C-C and C-H bonds interlaced, the appearance of the v_1 peak indicates the emergence of nanocrystalline structures [32], and the v_3 peak is caused by the stretching vibration of C=C, which embodies interplanar defects, and is more sensitive to interstitial atom-shaped defects in graphite, and amorphous carbon [33]. The insignificant intensity of the v_1 and v_3 peaks in unirradiated graphite indicates that only few interstitial atomic-type defects existed in the graphite before irradiation and that the graphite possesses a highly ordered microcrystalline structure. The trends of I_{v3}/I_G and I_D/I_G with irradiation dose as well as the changes in L_a of NSPG and IG-110 before and after ion irradiation are shown in Figure 7(f) and Table 3, respectively. The results show that the I_{v3}/I_G increases and then slowly decreases with irradiation dose after irradiation, which indicates that a large number of interstitial atoms are formed at the beginning of irradiation, and then the compounding of the interstitial atoms and vacancies may have occurred afterward. After irradiation at a dose of 0.1 dpa, the relative intensity as well as the FWHM of the D peak increased significantly, indicating that the irradiation led to a rapid increase in the defect density of the graphite. It is worth noting that the characteristic peaks of the graphite (D and G peaks) are still distinguishable at this dose, and the magnitude of the change in I_D/I_G is also small compared to that of IG-110, with the decrease of L_a from ~32 nm for the pre-irradiated to ~19 nm. This indicates that the defect density of NSPG increases relatively slowly and has a certain resistance to irradiation, the laminar structure of NSPG after irradiation remains within the scale of a dozen nanometers, and the microcrystalline graphite is decomposed into nanocrystalline graphite. As the irradiation dose was increased to 2.5 dpa and 5.0 dpa, the D and G peaks began merging due to broadening, while the size of L_a decreased from ~12 nm to ~9 nm (see Table 3). This was attributed to the rapid growth of defects that severely damaged the graphite base layer, leading to bending and deformation of the basal plane. As a result, the nanocrystalline graphite gradually transitioned towards amorphization, aligning with the conclusions drawn from GIXRD. Raman spectroscopy further corroborates this by providing evidence of lattice defects.

Table 3. Changes of L_a in NSPG and IG-110 graphite before and after ion irradiation.

Graphite	NSPG/IG-110				
Irradiation damage dose (dpa)	0	0.1	0.5	2.5	5.0
Crystallite Lateral Size L_a (nm)	31.516/24.976	18.664/8.339	11.581/7.633	9.423/7.542	9.111/7.267

 doi:10.20944/preprints202404.0876.v1

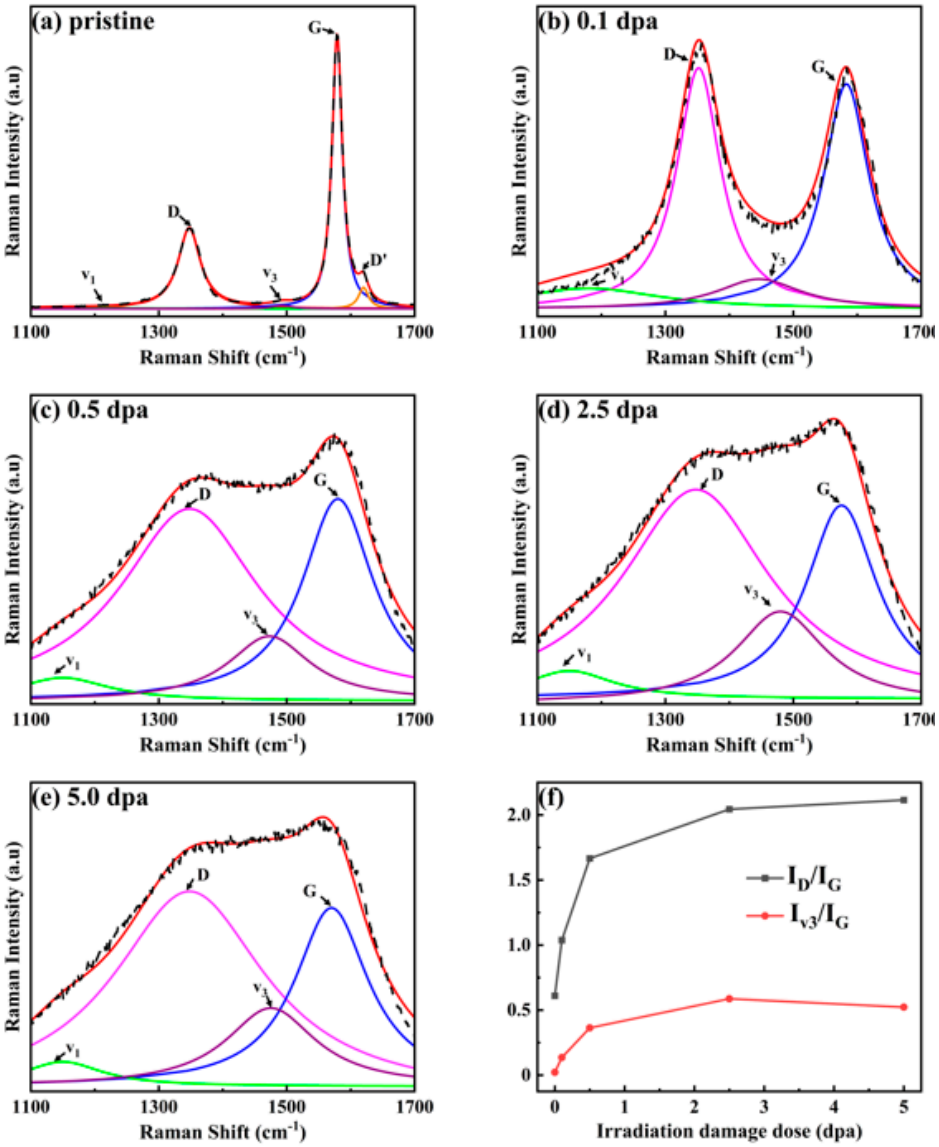

Figure 7. Raman spectra of NSPG (a) before and (b-e) after irradiation; All spectra were fitted with Lorentz line shape fitting. (f) I_D/I_G and I_{v3}/I_G as functions of irradiation dose.

4. Conclusions

In summary, the NSPG prepared by the "no impregnation" process can reduce the pore size of graphite to ~ 800 nm, which can meet the requirement of molten salt reactors. NSPG was screened using ion beam irradiation to simulate neutron irradiation. The results show that the graphitization degree of NSPG was better than IG-110. Under low-dose ion irradiation (<2.5 dpa), NSPG exhibits better resistance to irradiation than IG-110, with smaller changes in the microstructure. The microstructural changes can be explained by the XRD results, which indicate that the increasing interlayer spacing of graphite after irradiation causes the shrinkage and closure of micropores on the surface of graphite. The change of L_c, first increasing and then decreasing, is related to the irradiation-induced disordered structure, leading to the appearance of a "ridge-like" structure. Raman spectroscopy results show that the defect density of NSPG increases relatively slowly, and the laminar structure of graphite remains within the scale of a few dozen nanometers after irradiation at doses (<2.5 dpa). As the irradiation dose increased, the accumulation of defects resulted in the graphite developing towards amorphization, which is consistent with the case of IG-110. The research reveals NSPG has better irradiation resistance than IG-110 under ion implantation at room temperature. which provides theoretical support for the application of NSPG in molten salt reactors.

 doi:10.20944/preprints202404.0876.v1

But its performance and behavior may be different at neutron irradiation and higher irradiation temperatures, and should be subject to the next step of neutron irradiation screening.

Acknowledgments: This work was financially supported by the National Natural Science Foundation of China (No. 52072397); Institute of Coal Chemistry, Chinese Academy of Sciences (No. SCJC-XCL202209); DNL Cooperation Fund, CAS (DNL202012).

References

1. Serp, J.; Allibert, M.; Beneš, O.; Delpech, S.; Feynberg, O.; Ghetta, V.; Heuer, D.; Holcomb, D.; Ignatiev, V.; Kloosterman, J.L.; et al. The molten salt reactor (MSR) in generation IV: Overview and perspectives. *Prog. Nucl. Energy* **2014**, *77*, 308-319.
2. McCoy, H.E.; Beatty, R.L.; Cook, W.H.; Gehlbach, R.E.; Kennedy, C.R.; Koger, J.W.; Litman, A.P.; Sessions, C.E.; Weir, J.R. New Developments in Materials for Molten-Salt Reactors. *Nucl. Appl. Technol.* **1970**, *8*, 156-169.
3. Rosenthal, M.W.; Haubenreich, P.N.; Briggs, R.B. *The development status of molten-salt breeder reactors*; Tennessee: Oak Ridge National Laboratory, 1972.
4. Campbell, A.A.; Burchell, T.D. Radiation Effects in Graphite. In *Comprehensive Nuclear Materials*; 2020; pp. 398-436.
5. Song, J.L.; Zhao, Y.L.; He, X.J.; Zhang, B.L.; Xu, L.; He, Z.T.; Zhang, D.S.; Gao, L.N.; Xia, H.H.; Zhou, X.T.; et al. Preparation of pyrolytic carbon coating on graphite for inhibiting liquid fluoride salt and Xe^{135} penetration for molten salt breeder reactor. *J. Nucl. Mater.* **2015**, *456*, 33-40.
6. He, Z.; Lian, P.F.; Song, Y.; Liu, Z.J.; Song, J.L.; Zhang, J.P.; Feng, J.; Yan, X.; Guo, Q.G. Improving molten fluoride salt and Xe^{135} barrier property of nuclear graphite by phenolic resin impregnation process. *J. Nucl. Mater.* **2018**, *499*, 79-87.
7. He, X.J.; Song, J.L.; Xu, L.; Tan, J.; Xia, H.H.; Zhang, B.L.; He, Z.T.; Gao, L.N.; Zhou, X.T.; Zhao, M.W.; et al. Protection of nuclear graphite toward liquid fluoride salt by isotropic pyrolytic carbon coating. *J. Nucl. Mater.* **2013**, *442*, 306-308.
8. He, X.J.; Song, J.L.; Tan, J.; Zhang, B.L.; Xia, H.H.; He, Z.T.; Zhou, X.T.; Zhao, M.W.; Liu, X.D.; Xu, L.; et al. SiC coating: An alternative for the protection of nuclear graphite from liquid fluoride salt. *J. Nucl. Mater.* **2014**, *448*, 1-3.
9. Zhang, J.C.; Shi, J.L.; Zhao, Y.; Guo, Q.G.; Liu, L.; Feng, Z.H.; Fan, Z. Structural changes in four different precursors with heat treatment at high temperature and resin carbon structural model. *J. Mater. Sci.* **2012**, *47*, 5891-5899.
10. Zhao, H.C.; He, Z.; Liu, Z.J.; Song, J.L.; Tsang, D.K.L.; Zhang, H.Y. Self-sintered nanopore-isotropic graphite derived from green pitch coke for application in molten salt nuclear reactor. *Ann. Nucl. Energy* **2019**, *131*, 412-416.
11. Song, J.L.; Zhao, Y.L.; Zhang, J.P.; He, X.J.; Zhang, B.L.; Lian, P.F.; Liu, Z.J.; Zhang, D.S.; He, Z.T.; Gao, L.N.; et al. Preparation of binderless nanopore-isotropic graphite for inhibiting the liquid fluoride salt and Xe^{135} penetration for molten salt nuclear reactor. *Carbon* **2014**, *79*, 36-45.
12. Wang, T.; Li, H.; Shen, Q.; Li, K.; Li, W.; Song, Q.; Zhang, S. Dependence of mechanical properties on microstructure of high-textured pyrocarbon prepared via isothermal and thermal gradient chemical vapor infiltration. *Composites Part B: Engineering* **2020**, *192*.
13. Zhang, H.Y.; Cheng, J.X.; Lian, P.F.; He, Z.; Wang, Q.; Yu, A.; Song, J.L.; Tang, Z.F.; Liu, Z.J. Effects of irradiation on nano-pore phenol-formaldehyde resin infiltrated IG-110 graphite. *Nucl. Mater. Energy* **2022**, *32*.
14. Zhang, H.Y.; Lei, Q.T.; Song, J.L.; Liu, M.; Zhang, C.; Gao, Y.T.; Zhang, W.T.; Xia, H.H.; Liu, X.D. Direct characterization of ion implanted nanopore pyrolytic graphite coatings for molten salt nuclear reactors. *RSC Adv.* **2018**, *8*, 33927-33938.
15. He, Z.; Lian, P.F.; Guo, X.H.; Song, J.L.; Yan, X.; Liu, Z.J.; Song, H.H. Ultrafine-grained graphite prepared from filler of onion-like carbon spheres via a liquid mixing process for using in molten salt reactor. *J. Nucl. Mater.* **2021**, *547*.
16. Zhang, H.Y.; Song, J.L.; Tang, Z.F.; Liu, Z.J.; Liu, X.D. The surface topography and microstructure change of densified nanopore nuclear graphite impregnated with polyimide and irradiated by xenon ions. *Appl. Surf. Sci.* **2020**, *531*.

 doi:10.20944/preprints202404.0876.v1

17. Liu, M.; Zhang, W.T.; Song, J.L.; Zhang, H.Y.; Lian, P.F.; Gao, Y.T.; Zhang, C.; He, Z.T.; Liu, Z.J.; Zhao, M.W.; et al. Irradiation resistance study of binderless nanopore-isotropic graphite for use in molten salt nuclear reactors. *Nucl. Eng. Des.* **2018**, *335*, 231-240.
18. Li, P.D.; Lian, P.F.; Song, J.L.; Zhang, H.Y.; Cheng, J.X.; Wang, Q.B.; Liu, Z.J.; Tang, Z.F. Surface topography and microstructure changes of ultrafine-grained graphite prepared from filler of onion-like carbon spheres by Xe ions irradiation. *Radiat. Phys. Chem.* **2024**, *219*.
19. Zhang, H.Y.; Song, J.L.; Tang, Z.F.; He, Z.; Liu, X.D. The surface topography and microstructure of self-sintered nanopore graphite by Xe ions irradiation. *Appl. Surf. Sci.* **2020**, *515*.
20. Zhang, H.Y.; Cheng, J.X.; Song, J.L.; Yin, H.Q.; Tang, Z.F.; Liu, Z.J.; Liu, X.D. Topography changes and microstructural evolution of nuclear graphite (IG-110) induced by Xe^{26+} irradiation. *New Carbon Mater.* **2023**, *38*, 393-402.
21. Dickinson, J.M.; Shore, J.W. Observations concerning the determination of porosities in graphites. *Carbon* **1968**, *6*, 937-941.
22. Washburn, E.W. The dynamics of capillary flow. *Physical Review* **1921**, *17*, 273-283.
23. Arregui-Mena, J.D.; Worth, R.N.; Bodel, W.; März, B.; Li, W.; Campbell, A.A.; Cakmak, E.; Gallego, N.; Contescu, C.; Edmondson, P.D. Multiscale characterization and comparison of historical and modern nuclear graphite grades. *Mater. Charact.* **2022**, *190*.
24. Huang, Q.; Li, J.J.; Liu, R.D.; Yan, L.; Huang, H.F. Surface morphology and microstructure evolution of IG-110 graphite after xenon ion irradiation and subsequent annealing. *J. Nucl. Mater.* **2017**, *491*, 213-220.
25. Jiang, M.; Ammigan, K.; Lolov, G.; Pellemoine, F.; Liu, D. Porosity evolution in proton irradiated microfine-grained POCO graphite. *J. Nucl. Mater.* **2023**, *587*.
26. Heggie, M.I.; Suarez-Martinez, I.; Davidson, C.; Haffenden, G. Buckle, ruck and tuck: A proposed new model for the response of graphite to neutron irradiation. *J. Nucl. Mater.* **2011**, *413*, 150-155.
27. Manoj, B. Investigation of nanocrystalline structure in selected carbonaceous materials. *Int. J. Miner. Metall. Mater.* **2014**, *21*, 940-946.
28. Zhou, Z.; Bouwman, W.G.; Schut, H.; van Staveren, T.O.; Heijna, M.C.R.; Pappas, C. Influence of neutron irradiation on the microstructure of nuclear graphite: An X-ray diffraction study. *J. Nucl. Mater.* **2017**, *487*, 323-330.
29. Asthana, A.; Matsui, Y.; Yasuda, M.; Kimoto, K.; Iwata, T.; Ohshima, K.-i. Investigations on the structural disordering of neutron-irradiated highly oriented pyrolytic graphite by X-ray diffraction and electron microscopy. *J. Appl. Crystallogr.* **2005**, *38*, 361-367.
30. Mathew, S.; Chan, T.K.; Zhan, D.; Gopinadhan, K.; Barman, A.R.; Breese, M.B.H.; Dhar, S.; Shen, Z.X.; Venkatesan, T.; Thong, J.T.L. The effect of layer number and substrate on the stability of graphene under MeV proton beam irradiation. *Carbon* **2011**, *49*, 1720-1726.
31. Tuinstra, F.; Koenig, J.L. Raman Spectrum of Graphite. *J. Chem. Phys.* **1970**, *53*, 1126-1130.
32. Ferrari, A.C.; Robertson, J. Origin of the 1150 cm^{-1} Raman mode in nanocrystalline diamond. *Phys. Rev. B* **2001**, *63*, 121405.
33. Ferrari, A.C.; Robertson, J. Resonant Raman spectroscopy of disordered, amorphous, and diamondlike carbon. *Phys. Rev. B* **2001**, *64*, 075414.